Seventh Canadian Masonry Symposium
McMaster University
Hamilton, Ontario
June 4-7, 1995

BEHAVIOR OF INTERLOCKING MORTARLESS MASONRY UNDER COMPRESSIVE LOADS

Kang-Ho Oh [1], Harry G. Harris [2] and Ahmad A. Hamid [3]

ABSTRACT

The behavior of interlocking mortarless masonry under compressive loads is studied by directly comparing experimental and analytical results. The techniques used to obtain all the input data necessary for a nonlinear FEM modeling technique are described. A three-dimensional nonlinear finite element model has been proposed that was developed in the ANSYS general purpose FEM environment. The required FEM input data including uniaxial stress-strain relations, nonlinear localized contact stiffness, frictional behavior, and geometric properties were determined by extensive experimental investigation. Very good agreement between the deformational behavior of the physical and the FEM models has been achieved.

INTRODUCTION

Interlocking mortarless or dry stacked masonry construction as an alternative to conventional block masonry with mortar joint construction shows great economic potential. The attractiveness of increased construction efficiency with potentially less skilled labor and thus lower costs accounts for the worldwide interest that has been shown for this new masonry construction technique [Glitza (1991), Harris et al. (1993)].
Two interlocking masonry blocks, namely the Modified-H and the WHD (Whelan-Hatzinikolas-Drexel) Blocks have been developed by the authors. Whelan (1985) laid the groundwork and Hatzinikolas (1991) suggested a geometric configuration that became the

1 Director of Research and Development, Hoon Ho Oh Builders, 810 South 53rd Street, Philadelphia, PA 19143, USA.
2 Professor, Department of Civil and Architectural Engineering, Drexel University, Philadelphia, PA 19104, USA.
3 Professor and Head, Department of Civil Engineering, United Arab Emirates University. On leave from Drexel University, Philadelphia, PA 19104, USA.

WHD Block developed by the writers and used in this study. A similar configuration came to the attention of the writers after they had evolved the geometry of their WHD Block. The interlocking masonry systems developed by the writers were investigated experimentally for their basic structural performance which was reported elsewhere [Harris et al. (1992), Harris et al.(1993), Oh et al. (1993), Oh (1994)]. Failure mechanisms of interlocking systems under compressive, shear, and flexural loading were also discussed based on the experimental evidence obtained. The structural behavioral differences of the interlocking masonry systems, as compared to the conventional masonry, that were obtained [Harris et al. (1993)] actually comes from the single fact, i.e., lack of filler material at the block-to-block interface. Although grout and surface bonding may greatly stabilizes the finished dry stacked masonry system, the block-to-block contact behavior at the block interfaces still is a vital contributor under various loading conditions. In the case of dry stacked masonry, the interface behavior at the dry bed joint is more complicated, as compared to the conventional masonry, due to the unavoidable air space in the initially un-contacted area. Gradual closing-up of the air space under load, known as 'seating' turns the interlocking mortarless masonry into a progressive contact problem. Although the interlocking mortarless masonry system is not new, no reported masonry research has been found which especially focused on this problem.

A microscopic finite element method approach was used to address this problem. Material and geometric properties of the WHD block were investigated experimentally to determine the input data required for the FEM modeling of the dry stacked masonry. Analytical models of the dry stacked masonry system using the FEM technique were developed. The ANSYS 5.0 general purpose finite element analysis package was chosen for this purpose. Simulation of the behavior of hollow dry stacked masonry under compressive loading was studied and, in particular, the effect of geometric imperfections at the block-to-block interfaces to the compressive deformation behavior were taken into account. The experimental results and the results of the FEM analysis of the dry stacked masonry under compressive load were compared.

The units of the WHD Block system are shown in Fig. 1(a) and (b). Interlocking of the end lugs provides horizontal and vertical bending rigidity prior to grouting. The method of reinforcement is shown in Fig. 1(c). Note that this requires "threading" of the units onto the vertical reinforcing bars but the system can be easily reinforced in the horizontal direction, see Fig. 1(c). The method of stacking and grouting is shown in Fig. 1(d). A geometric scale of 1/3 was chosen to facilitate the development of the new block.

FEM INPUT DATA

Stress-Strain Relationship

Because the density distribution of the material in the individual WHD Blocks was not perfectly uniform, it was necessary to make several different types of block coupons cut out from different parts of the WHD Blocks to obtain reliable stress-strain data for input into the FEM analysis. Figure 2 shows the four types of compressive coupons tested. Block coupons Type I and Type II were cut out from the faceshell of the WHD Blocks. Because of the small faceshell thickness (11.7 mm) and noticeable damage during saw cutting the desirable square cross section could not be made for those coupons shown in Fig. 2. Block coupons Type III

and IV were taken from the relatively thick external web of the WHD Blocks. Square cross sections were reasonably achieved for these coupons.

A total of 100 coupon samples were taken from the WHD Blocks and tested. Forty-six specimens were tested to obtain the stress-strain relations and the rest were tested for compressive strength only. Specimens were capped with Hydrostone, a high strength gypsum compound. Due to the small size of the coupon specimens, LVDT's could not be installed on the specimens directly. A bearing block equipped with 4 spring loaded LVDT's was specially developed to facilitate the coupon testing as shown in Fig. 3. This device indirectly measures overall longitudinal deformation of a coupon specimen that is placed between the top and bottom loading blocks, see Fig. 3. Therefore, it is important to make both surfaces of capping and bearing blocks as smooth as possible to provide air tight contacts. For this reason, the top surface of steel blocks was specially treated by precision milling.

The average curves of each type of coupon test are compared in Fig. 4. Due to the unknown density distribution, size effect, and platen effect, it is not possible to separate what contribution each of the variables has on the stress-strain behavior. Likewise, it is not possible to directly derive the real uniaxial stress-strain relation from the physical tests. However, with a known stress-strain relation and the actual boundary conditions used in the test, it is possible to identify the required FEM material parameters inversely which is known as the 'inverse identification approach'. The material behavior was modeled based on the averaged stress-strain relation of specimens Type I using the aforementioned approach. Stress-strain relations obtained from the tested Type II, Type III, and Type IV coupons were used for verification of the established material model.

Contact Behavior at Dry Stacked WHD Block Bed Joint

When concrete blocks are stacked without filler material, they are still in contact via roughness, texture, etc. (named herein 'virtual filler') rather than the material properties of the block units themselves. Therefore, it is necessary to determine the stiffness of the 'virtual filler' to properly model dry stacked masonry. This requires the contact area of the joint specimen sufficiently small so that the progressive contact behavior of the overall curvature is minimized. Furthermore, to eliminate the undetermined contribution of the material deformation, direct measurement at the dry joint is necessary. A typical test setup to measure the contact stiffness at the dry stack joint using a specially fabricated clip gage is shown in Fig. 5. Load was applied via a ball bearing placed at the center of a 6.4 mm thick bearing block to assure uniform transfer of the load. Very slow rate of displacement was applied to the specimen specially in the beginning to capture the rapidly increasing contact stiffness at the interface. Average load-deformation relation obtained by this technique is shown in Fig. 6. The slope of the curve represents the local contact stiffness of the dry stacked masonry.

Friction at Dry Stacked WHD Block Bed Joint

The objective of this test was to obtain local coefficients of friction at the dry stacked masonry bed joint. Three pieces of block coupons were cut from the faceshell of the WHD Blocks and arranged in such a manner to simulate the possible sliding at the dry stacked bed joint. Test setup and boundary conditions provided are shown in Fig. 7. As can be seen in the figure, lateral precomression forces are applied to the specimen via bearing pins to generate uniform normal stress normal to the test joints. Double shearing stresses parallel to the test

joint are induced by the vertical displacement continuously applied on the center piece of the specimen by the spherical loading head .
Table 1 summarizes peak shear forces monitored at different precompression levels. Coefficients of friction calculated based on these values are also shown in Table 1.

Geometric Imperfection of the WHD Block Bed Joint
Unlike conventional masonry, the geometric properties at the bearing surfaces plays a vital role for dry stacked masonry. Precisely fabricated dry stacking masonry blocks not only improve the structural performance but will assure faster construction and better wall alignment. In order to measure more accurate geometrical properties (several hundredth of a mm of variation), an experimental technique was developed as described below. Four LVDT's were used to scan three-dimensional geometric properties of the block at the locations shown in Fig. 8. The tip of each LVDT core was modified by installing a sliding shoe made of a thin brass plate. A milling machine work bed was used to feed test blocks at a controlled rate as shown in Fig. 9. Typical scanned curvatures using the 4 LVDT's of Fig. 9 are shown in Fig. 10.
Actual gap size at the dry stacked masonry is not easily determined from only the scanned curvatures. Therefore, direct measurement was also made using a conventional gap gage. Gap sizes varied mostly in a range from 0.03 to 0.15 mm.

FINITE ELEMENT METHOD MODELING

Constitutive Relationships
The nonlinear stress-strain relationships of the block and the grout materials were simulated by combing the Drucker-Prager yield criteria (ANSYS: D-P option) and the Rankine failure criteria (maximum principal stress theory), see Fig. 11. An inverse identification procedure was used for determination of the required input parameters. The inverse identification procedure was used because the required input parameters such as uniaxial yield stresses can not be determined from the physical tests. This is because the test boundary conditions and the size effect associated with heterogeneous characteristics of concrete-like materials violate the assumptions made for the FEM model. Therefore, iterative FEM analyses with actual test boundary conditions were carried out until the FEM result reasonably matched the physical test results. Failure was predicted by comparing the maximum principal stresses in the FEM prism model at each load increment to the material uniaxial strength. The methodology of combining a yield criteria and a fracture criteria is known as the plastic-fracture approach. The Drucker-Prager yield criteria assumes elastic-perfect plastic behavior (in both compression and tension) under a pure uniaxial state of stress. When a FEM model is subjected to multiaxial states of stress, progressive material yielding will result. This implies that the analyses should be iterative and a trial yield stress should be input to the FEM model with actual test boundary conditions whose results are already known. The yield surface is a circular cone with the material parameters chosen such that they correspond to the outer aspices of the hexagonal Mohr-Coulomb yield surface, Fig.

11. The required data for the Drucker-Prager plasticity are: cohesion value c, the angle of internal friction ϕ, and the dilatancy angle ϕ_f

Verification Analysis

The FEM material model was verified by comparing the analytical stress-strain relationship to that obtained from coupon tests Type II, Type III, and Type IV specimens (Fig. 2). Configuration of these FEM models is shown in Figs. 12. The shaded area in Fig. 12 indicates the portion FEM modeled. The input material parameters determined remained the same and only specimen dimensions were varied according to the actual sizes of those coupon specimens. Stress-strain relations calculated by the FEM model are compared to those from corresponding test curves. Generally, good agreement was obtained for all the comparisons. Typical results for Type II coupons are shown in Fig. 13.

Dry-Stacked Prism

To closely simulate the nonlinear contact behavior observed, a three-dimensional surface-to-surface contact element (ANSYS: CONTAC52) was selected and was combined with a nonlinear spring element (ANSYS: COMBIN39) as shown in Fig. 14 (a). A nodal degree of freedom coupling technique was used on nodes 'i' and 'j' to allow only one directional (longitudinal) displacement of these nodes. The resulting normal stiffness response between nodes 'i' and 'k' is shown in Fig. 14 (b).

In the direction parallel to the bed joint, an elastic Coulomb friction behavior was assumed. The resulting frictional response is shown in Fig. 14 (c) where the slope denotes shear stiffness at the contacting surfaces and μ indicates the coefficient of friction that was obtained from the tests, see Table 1.

A compatible FEM dry stacked hollow masonry prism similar to those tested in the present study was modeled using the finite element method with the material and contact nonlineariry models developed as shown in Fig. 15. For the masonry block, the 8 noded 3-D solid element (ANSYS: SOLID45) was used which was implemented with the Druker-Prager plasticity material model developed. For the loading plate, the 8 noded 3-D solid element (ANSYS: SOLID45) with assigned elastic properties was used. Dry joints were simulated by combining,the 3-D contact element (ANSYS: CONTAC52) and the nonlinear spring element (COMBIN39) as previously described. Due to the asymmetry of the gap size, the whole 4-course 3-joint masonry prism was modeled. To maintain the recommended element aspect ratio (aspect ratio < 2) and to simulate progressive gap closing behavior, a relatively fine mesh was unavoidable as shown in Fig. 15. The material parameters used for the Druker-Prager plasticity model were: 1) Modulus of elasticity =9.228 GPa; 2) Poisson's ratio = 0.2; 3) Druker-Prager yield criterion: cohesion= 1.524 MPa; internal friction= 60.60°; and, dilatancy angle= 30°.

A total load of 4.448 KN was applied at an increment of 556 N. At each load increment maximum of 40 equilibrium iterations were allowed. Typically solution converged in 7 to 13 equilibrium iterations. No sliding was assumed at both top and bottom where the Hydrostone capping is isolated as it most probably occurs in the physical test.

RESULTS AND CORRELATION

Stress-strain relation

The stress-strain relation obtained from the FEM model is compared to the test results and the material stress-strain relation input in Fig. 16. Strain was calculated as longitudinal deformation across 3 courses and 2 dry joints divided by the gage length. Stress was calculated as the total load applied divided by the net loaded area. The same procedure was used in calculating the test stress-strain relations. As can be seen in Fig. 16, a good agreement is achieved between strain-stress relations of the FEM and physical models.

Initial Seating Behavior

The unique progressive seating of dry stacked masonry followed by the reduced stiffness and the peak stress was reproduced by the FEM model. Figure 17 compares the initial progressive contact behavior (seating) of the FEM and the physical model. The initial seating strain (ε_o) of 0.0006 predicted by the FEM model compares very well with the strain of 0.0005 obtained from the test.

Modulus of Elasticity

The input elastic modulus of the material of 9.228 GPa was reduced to 5.172 GPa by the 3 course stack prism FEM model. The loss of the elastic modulus in the dry stacked hollow masonry is due to the complex combined effect of the material and contact nonlinearity. The reduction predicated by the FEM model also compares very well with that obtained from testing of the physical models which gave an average modulus of elasticity of 4.752 GPa from 6 prism tests.

Stress Distribution

Typical results of the FEM model analysis are shown in Fig. 18 which shows the maximum compressive stress distribution in the 3 course stack prism. As can be seen in Fig. 18, the analysis shows an asymmetric stress distribution with peak values near the compressive strength of the block material.

CONCLUSIONS

A successful interlocking masonry system is dependent on the geometric accuracy and repeatability, especially the height, achieved in the interlocking block. The peak strength achievable by the dry stacked hollow masonry is dependent upon the degree of imperfection at the bed joint surface. Ideally, strength can approach up to or near the material strength with securely seated mortarless masonry. The characteristics of the surface condition of bearing area including roughness, hardness, degree of local curvature (previously called 'virtual filler') will control the forgiveness of the global geometric imperfections. For example, lower stiffness virtual filler better facilitates gap closing at the same load level than does a stiffer 'virtual filler'. The deformation of the virtual filler is considerable only in the initial loading stage. As the load increases, the contribution of the 'virtual filler' to the component stiffness

reduces greatly. Surface bonding or post tensioning will improve masonry performance greatly. In the case of surface bonding, however, tensile as well as compressive stress will essentially be resisted by the surface bonding material. Therefore, the problem of bulging and/or debonding should be carefully considered. Stiffness reduction comes from stress redistribution due to poorly distributed tensile and compressive stresses in the block. Therefore, the nature of the failure mode is rather brittle as compared to conventional masonry. The degree of the stiffness reduction is therefore greatly controlled by the degree of the geometric imperfection.

ACKNOWLEDGMENT

The authors appreciate the support received from the National Science Foundation through Grant No. MSM-9102769.

REFERENCES

1. Anonymous, (1992), "ANSYS User's Manual for Revision 5.0," Vol. IV, Theory, Swanson Analysis Systems, Inc., Houston, PA 15342.
2. Anonymous, (1993), "ANSYS- Structural Nonlinearities, User's Guide for Revision 5.0," Swanson Analysis Systems, Inc., Houston, PA 15342.
3. Crofts, F.S. (1993) "State-of-the-art of Mortarless Concrete Masonry in South Africa," Proceedings, The 6th North American Masonry Conference, Drexel University, Philadelphia, Pennsylvania.
4. Gliza, H. (1991), "State-of-the-art and Tendency of Development of Masonry Without Mortar," Proceedings of the 9th International Brick/Block Masonry Conference, Berlin, Vol. 2, pp. 1028-1033.
5. Harris, H.G., Oh, Kang-Ho, and Hamid, A.A. (1992) "Development of New Interlocking and Mortarless Block Masonry Units for Efficient Building Systems," Proceedings of the 6th Canadian Masonry Symposium, Saskatoon, Saskatchewan, Canada, Vol. 2, pp. 723-734.
6. Harris, H.G., Oh, Kang-Ho, and Hamid, A.A. (1993) "Development of New Interlocking Blocks to Improve Earthquake Resistance of Masonry Construction," Report to the National Science Foundation, Department of Civil and Architectural Engineering, Drexel University, Philadelphia, Pennsylvania, 146p.
7. Hatzinikolas, M.. (1991), Prairie Masonry Institute, Edmonton, Alberta, Canada, Private Communication.
8. Oh, Kang-Ho (1994) "Development and Investigation of Failure Mechanism of Interlocking Mortarless Block Masonry Systems," Ph.D. Thesis, Department of Civil and Architectural Engineering, Drexel University, Philadelphia, Pennsylvania.

9. Oh, Kang-Ho, Harris, H.G., and Hamid, A.A. (1993) "New Interlocking and Mortarless Block Masonry Units for Earthquake Resistance Structures," Proceedings, The 6th North American Masonry Conference, Drexel University, Philadelphia, Pennsylvania, Vol. 2, pp. 821-836.

10. Whelan, L. (1985) "Hollow Concrete Masonry Unit Shape Modification to Improve Productivity of Placement: Results of the Primary Research Effort," Proceedings of the 3rd North American Masonry Conference, University of Texas, Arlington, pp. 9-1 to 9-8.

Table 1 Joint Friction Test Results.

	Normal Force (N)	Shear Force at peak (N)	Shear Force sliding (N)	Coef. of Friction (at peak)	Coef. of Friction (sliding)
	347	565	556	0.82	0.80
	445	827	756	0.93	0.85
	507	925	881	0.91	0.87
	761	1,334	1,290	0.86	0.83
	921	1,690	1,646	0.90	0.87
	1,232	2,335	2,313	0.92	0.92
Mean	NA	NA	NA	0.89	0.85
S.D.				0.04	0.04
COV (%)				4.7	4.76

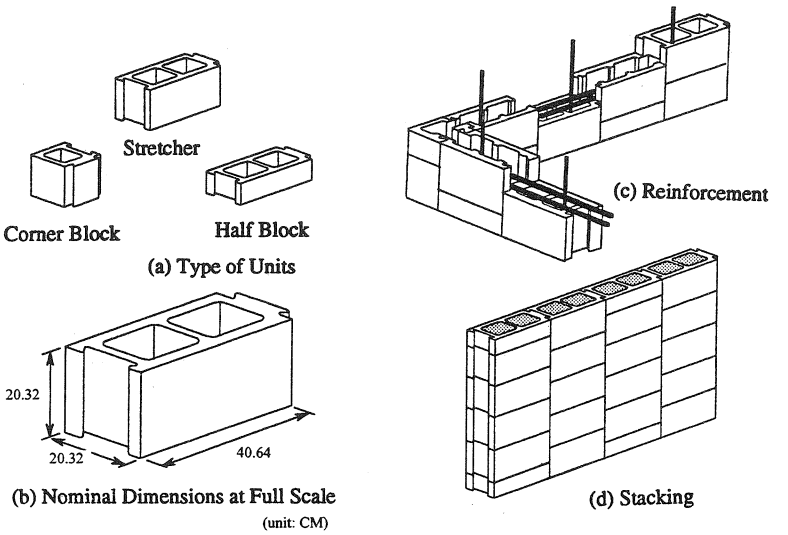

Fig. 1 WHD Block Masonry System.

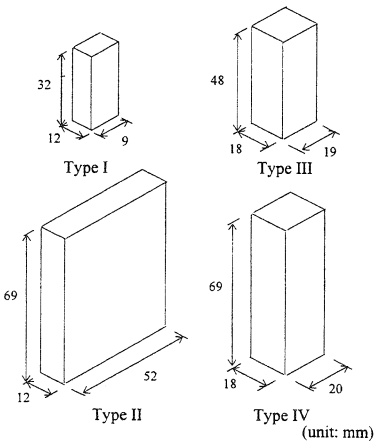

Fig. 2 Configurations of Block Coupon Samples.

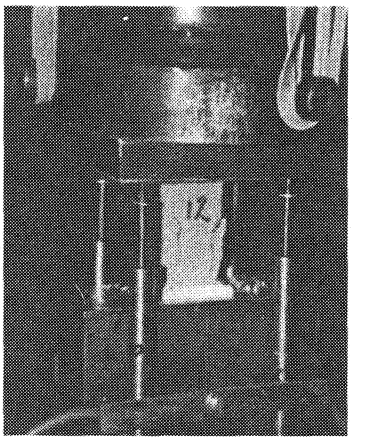

Compressive Load.

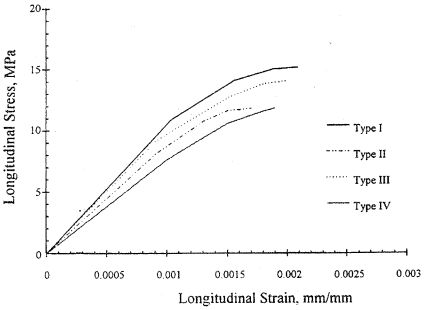

Fig. 4 Averaged and Segmented Stress-Strain Curves of Coupons Tested.

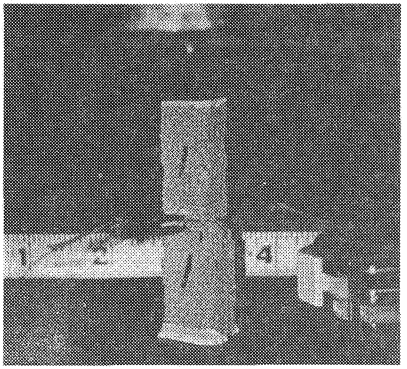

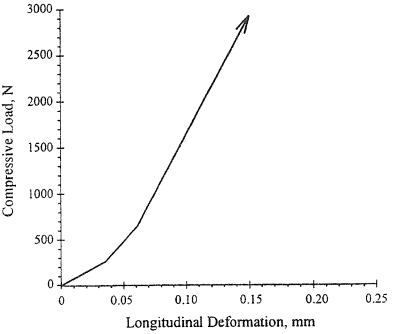

Fig. 6 Nonlinear Local Contact Stiffness.

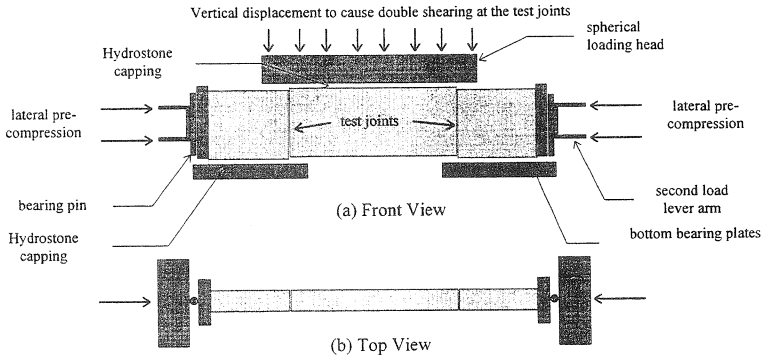

Fig. 7 Joint Friction Test Setup.

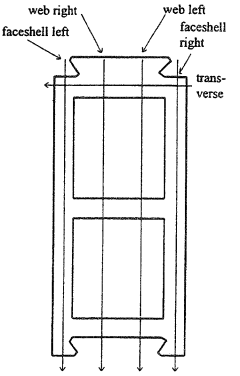

Fig. 8 Paths of Bed Joint Scanned.

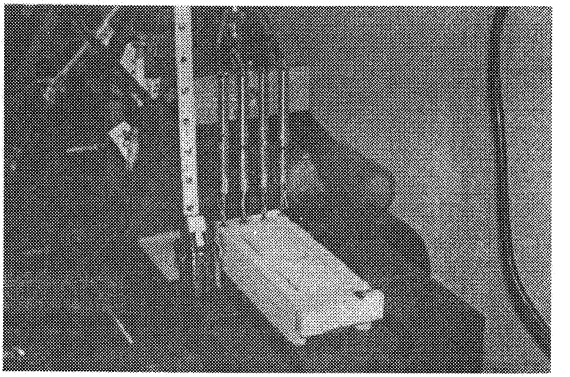

Fig. 9 A WHD Block Being Scanned for Bed Joint Level.

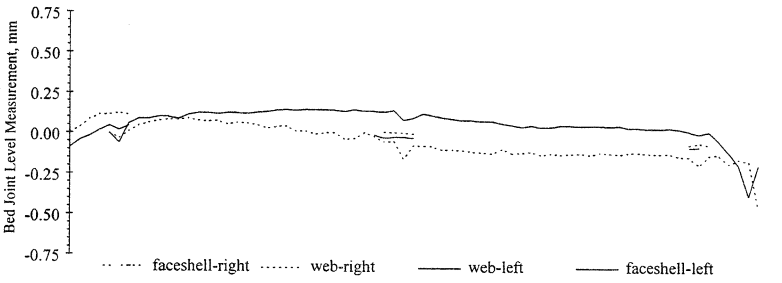

Fig. 10 Typical Result of Bed Joint Surface Level Scanned.

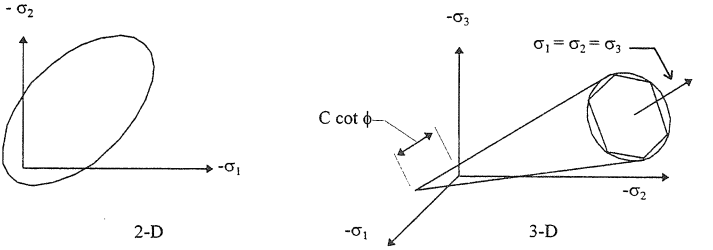

Fig. 11 Drucker-Prager and Mohr-Coulomb Yield Surfaces.

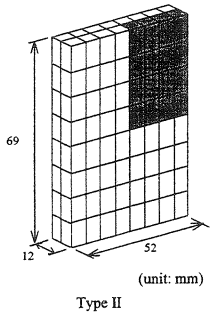

Fig. 12 Verification Model Type II Showing FEM Mesh.

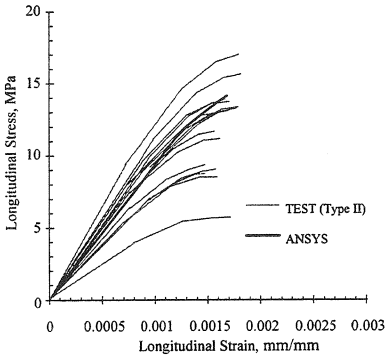

Fig. 13 Comparison of Analytical and Experimental Stress-Strain Relations for Coupon Type II.

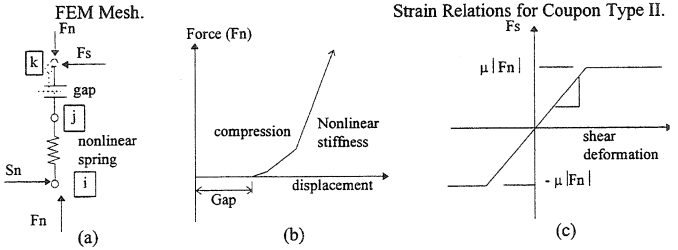

Fig. 14 Combined Contact Element and Stiffness Responses Normal and Parallel to the Bed Joint.

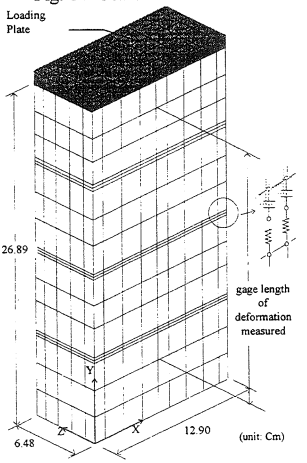

Fig. 15 FEM Model for Dry stacked Prism.

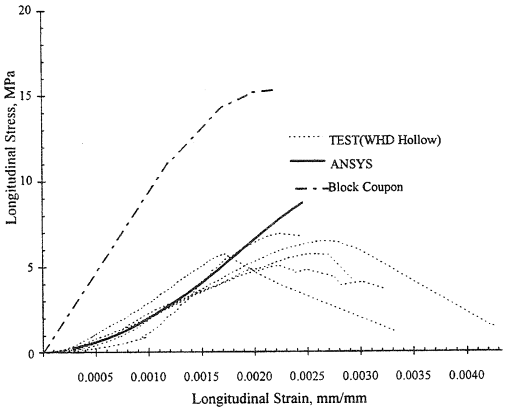

Fig. 16 Comparison of FEM and Physical Model Results for Stress-Strain Relations.

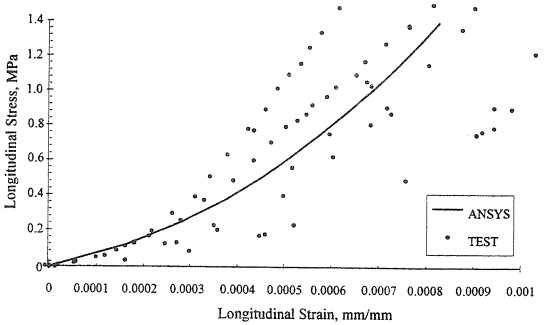

Fig. 17 Initial Seating Behavior of FEM Analysis and Experimental Results.

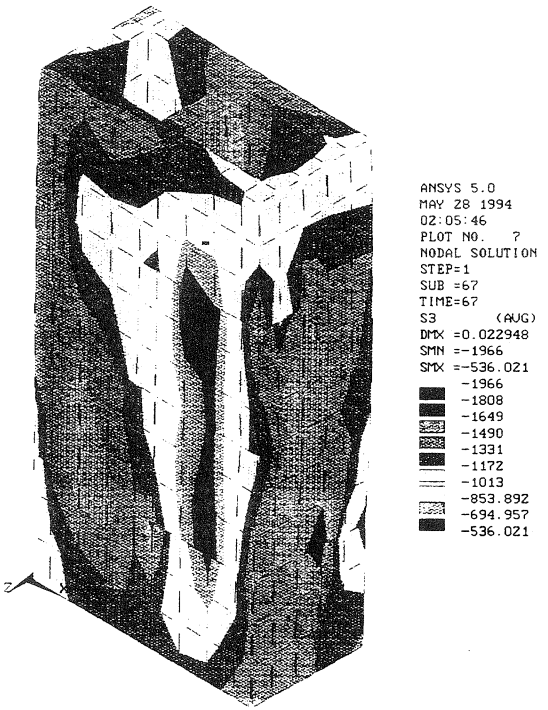

(145 psi= 1 MPa)

Fig. 18 Maximum Compressive Principal Stress Distribution in High Load Level (Hollow Prism).